Energy & Buildings 263 (2022) 112024

Contents lists available at ScienceDirect

Energy & Buildings

journal homepage: www.elsevier.com/locate/enb

Characterization of a naturally ventilated double-skin façade through the design of experiments (DOE) methodology in a controlled environment

Aleksandar Jankovic, Francesco Goia *

Department of Architecture and Technology, Faculty of Architecture and Design, Norwegian University of Science and Technology, NTNU, Trondheim, Norway

ARTICLE INFO

Article history:
Received 28 December 2021
Revised 23 February 2022
Accepted 10 March 2022
Available online 11 March 2022

Keywords:
Design of experiments
Analysis of variance
Climate simulator
Double-skin facades
Airflow
Thermal behavior

ABSTRACT

The two-fold aim of this study was to compare and reflect on the impact of different experimental designs on the characterization of a complex façade system, and to understand the role of constructional elements and boundary conditions on the thermal and fluid dynamic behavior of a double-skin facade (DSF), focusing on the controllability of these phenomena during the operation of the DSF.

We employed and compared four experimental designs capable of assessing factors' interactions and non-linear behaviors typical of dynamic façades. Experimental data were obtained using a full-scale DSF mock-up, installed in a climate simulator, which was operated in outdoor air curtain mode under boundary conditions typical of the summer season. Similarities and differences between characterizations obtained through different experimental designs enabled us to analyse the impact of different experimental designs and to identify the features that affect the DSF's performance.

The results demonstrated that the design of experiments methodology could be successfully employed to study the behavior of complex facades. Using more than one experimental design allowed us to obtain a robust picture of the behavior of a naturally ventilated façade. Relevant factors and interactions were also identified and linked to phenomena that determine how the DSF behaves under typical summer conditions.

1. Introduction

1.1. Background

Thermal and energy performance of double-skin facades (DSFs) are linked to non-linear behaviors driven by the boundary conditions and controlled by the structural elements and operational modes. As opposed to the influence of a single factor, the combined effects of multiple factors, such as the simultaneous balance between different driving forces or the interaction of different constructional features, are challenging to understand and are rarely analyzed [1]. The design of experiments (DOE) represents an efficient and reliable method, based on well-established statistics theories [2], to systematically quantify and classify impacts of factors and their interactions in complex systems, as a DSF is. Each DOE begins with the problem statement, followed by establishing the objectives, which then determine the performance indicator (response quantity) and affecting factors to be studied [3]. A crucial step in the whole course is the selection of one (or more) suitable experimental design (also called an array) [4]. Experiments are executed according to the designed array once the experimental design(s) is chosen [5]. In the final stage, the analysis of variance (ANOVA) and other associated statistical methods are used to analyze the collected data to understand the impact of each factor (and sometimes their interactions, too) on the response quantity(s) [6].

There are few examples of DOE methodology in building energy or thermal performance research, and most focus primarily on numerical experiments (simulations) [7]. Some research activities use impact analysis to obtain performance characterization [8,9], while others employ DOE for optimization [10,11]. There are also examples where building simulations were paired with the DOE approach to find the optimal experimental design [12,13] and to develop a simple surrogate model [14].

Adopting the DOE method implies systematically altering several factors across experiental runs [12,15] with the aim of obtaining a full characterization with the least possible amount of experimental tests. The choice of experimental design(s) is not trivial, as not all those available are well-suited to characterize a given phenomenon. Depending on the nature of the studied process, some arrays may be too shallow to recognize the full complexity of the process. Consequently, they can provide incorrect

* Corresponding author.
E-mail address: francesco.goia@ntnu.no (F. Goia).

https://doi.org/10.1016/j.enbuild.2022.112024
0378-7788/

Nomenclature

Acronyms

2-FI	2-factor interaction model
ANOVA	Analysis of variance
BIG	Big size of the opening
CCD	Central composite design
DBT	Temperature difference
DOE	Design of experiment
DSD	Definitive screening design
DSF	Double skin facade
F	Factor
FFD	Full factorial design
H	Height
ISR	Solar irradiance
L	Level
MID	Mid-size of the opening
OFF	Raised venetian blinds (no shading)
OS	Opening size
RQ	Research question
RSD	Response surface design
SA	Slat angle
SMALL	The small size of the opening
TD	Taguchi design
W	Width

Symbols

c	Contribution [%]
f	Fitting coefficient [–]
k	Number of factors [–]
q	Heat flux density [Wm^{-2}]
SS	Sum of squares [same as for the response quantity]
t	Temperature [℃]
v	Velocity [ms^{-1}]
V	Airflow rate [m^3h^{-1}]

Subscripts

cav	refer to cavity
D	refer to the compared design
E	refer to error
F&I	refer to factor or interaction
net	refer to net
RD	refer to referent design
s	refer to indoor surface
T	refer to total
vent	refer to ventilated

or partially incorrect conclusions on the importance of particular factors and the extent of non-linearity within the process. Therefore, the experimental design(s) need to be well chosen to consider all non-linearities and the interaction of factors in the investigated process. For complex behavior dictated by several factors in a non-linear way, such as the thermal and fluid-dynamical behavior of a DSF, the use of experimental designs that can assess interactions (so-called arrays with resolution ≥IV [16]) is mandatory as they are the only ones capable of considering the how two or more factors in combination affect the response quantity. However, the complexity and comprehensiveness of experimental designs often need to be carefully balanced against the costs and duration of the experimental runs. In short, the struggle is to find the most comprehensive system characterization using the fewest resources possible.

In a previous study where we employed extensive simulations to create the dataset for analyses, we investigated how the DOE could be applied to a complex system such as a mechanically-ventilated DSF [12] for a complete characterization of its performance. We compared more than 30 different arrays to define guidelines for finding an optimal experimental design that would give the most comprehensive picture of the process, including all non-linearities, using the fewest resources possible.

Building on that theoretical, simulation-based investigation, we have now examined how well the characterization of the DSF performance can be carried out using real experiments in a laboratory setting, following the guidelines we have developed, through the application of some of the most promising experimental designs. This examination has allowed us to obtain a comprehensive picture of the thermophysical and fluid dynamic behavior of a naturally ventilated DSF.

2. Research aims, research questions, and audience

The study we present in this paper aims, at first, to examine how a laboratory characterization based on a certain experimental design may differ from another based on a different experimental array. We also hypothesize that by comparing the results obtained with more experimental designs, one can obtain robust knowledge about the behavior of the tested DSF, which is the second aim of this paper. The research questions that drove the development of this study were:.

RQ1) Do different experimental designs give the same characterization picture, and what features should an experimental design have to characterize the complex systems/processes of a DSF adequately?

RQ2) What is the thermophysical and fluid dynamics behavior of a naturally ventilated DSF under summertime conditions?

RQ3) What factors and their interactions effect (and how) the heat transfer and air dynamics in a DSF?

By answering the research questions, we also aim to validate the approach previously developed with the assistance of simulations on selecting suitable arrays and deepen our understanding of the complex DSF behavior in terms of its thermal and fluid-dynamics processes. We employ a flexible experimental testbed that we have previously developed [17]. This experimental facility makes it possible to carry out thermal and fluid mechanical characterization on DSF configurations in a laboratory setting. The experimental testbed consists of a flexible mock-up with operable features (such as cavity depth, venetian blinds angle, airflow path, airflow rate, opening size), a climate simulator, and a real-time control system experiment and data acquisition.

The results of this study can guide experimental researchers investigating the overall behavior of a complex system/phenomena/process in a wide range of conditions to find the most efficient way to reach their goals. Moreover, the results of the experimental campaign (with almost fifty different configurations of a DSF tested in response to various boundary conditions) are made publicly available for the scientific community for future independent research and calibration and validation of numerical models. Furthermore, by carrying out the study on a particular type of DSF, the results of this study also contribute to deepening the knowledge of the thermal and fluid mechanical behavior of naturally ventilated DSFs.

The contents of the papers are organized as follows. After this brief introduction, we describe, in the section ‘‘Methods and materials,” the overall research design and objectives; we provide general information on the DOE methodology, and more specifically, its application to the case study DSF. In the ‘‘Results and discussion” section, we present and compare the characterization outcomes for the different experimental designs. Based on the common features, we draw overall conclusions on the thermal and fluid dynamics behavior of DSF. Finally, in the ‘‘Conclusion” section, we summarize the outcomes related to the impact of different experimental designs, and we set our findings of the thermophysical and fluid mechanic behavior of a DSF in the context of the current knowledge in this domain.

3. Materials and methods

3.1. Research design and research objectives

In this research, we used the design of experiment (DOE) methodology to study, in a laboratory setting, the behavior of double-skin facades (DSFs), with a two-fold aim: to compare and reflect on the impact of different experimental designs (i.e., whether or not they provide the same outcomes), and to understand the role of construction elements and boundary conditions on the overall thermal and fluid-dynamics phenomena in DSF (i.e., how different features in a DSF impact on its performance). The methodological approach we adopted in this investigation was broken down in a series of steps that are described by the following research objectives:.

1) To identify a suitable case study (i.e., a DSF configuration), representative boundary conditions, and a set of performance parameters that describe the behavior of the DSF to be characterized.
2) To select several experimental designs based on previously defined guidelines that could be suitable to characterize the performance of the DSF.
3) To carry out a series of experimental runs, based on the arrays identified in the previous step, using a flexible DSF mock-up installed in a climate simulator.
4) To analyze the data collected during the various experimental runs by adopting the DOE methodology, in order:
   a) to compare the characterizations obtained through different arrays in both a quantitative and qualitative way – to be able to answer RQ1.
   b) to identify common patterns in the characterizations obtained with different arrays that can allow one to describe with a good degree of confidence the overall thermal and fluid-dynamical behavior of the DSF –to be able to answer RQ2.
   c) to analyze the impact of the different factors and their interactions in determining the DSF behavior – to be able to answer RQ3.
5) To synthesize the conclusions and main implications of the study in regards to:
   a) the use of different experimental designs in the characterization of a complex system such as a DSF;
   b) the impact of operational features and boundary conditions on the performance of a DSF.

3.2. The design of experiment (DOE) methodology

The performance of a DSF (and, in general, of a complex system) may depend on many factors (either constructional features, operational features, or boundary conditions) and their multiple interactions. It is practically impossible, in most cases, to investigate all the possible combinations of such factors with real experiments, as this would require unlimited resources in terms of time and costs. The DOE methodology mitigates these limitations because it reduces the number of experiments to be carried out so that the obtained characterization picture is as close as possible to the one acquired by running all the possible combinations. The selection of an experimental design (or array) is at the heart of the DOE methodology, and one has the possibility to choose among a large number of possible arrays, built by using different logics and different statistical theories. In this investigation, we selected four classes of experimental designs that are most often employed for characterization in different engineering fields [18]. The classes of experimental design we decided to employ in this study are synthetized below, and the selection of the exact design features within each class was based on the experience gained and the guidelines developed in a previous study [12].

***Taguchi design* (TDs)** has become the most applied experimental design in science and industry [19,18] even though it shows some limitations [20] because of its high flexibility in combining factors with different levels using few experimental runs [21]. The resolution of TDs varies from the most simple ones intended for screening to more complex ones designed for in-depth characterization.

Definitive screening design (DSD) is intended for screening in combination with two-factor interaction assessment. The advantage of this array is that it lowers the required experimental runs to $2 \cdot k + 1$ (k number of factors) [22]. Its application comes in handy for the processes driven by many factors or in situations where it is desired to filter the most important ones.

Full-factorial design (FFD) contains all possible combinations of the factors and corresponding levels and can provide a more profound characterization picture than any other experimental design [4]. Since it considers all possible combinations, the number of experimental runs grows significantly with the increase of factors or levels.

Central-composite design (CDC) offers a comprehensive understanding, and it is most commonly applied for optimizing system performance, when the number of factors is narrowed by some screening method to five or lower. CCD can assess higher-order terms and the curvature in the response of the output quantity [23].

After performing the experimental runs using the selected array (s), the collected data are post-processed using regression analysis and the analysis of variance (ANOVA). The regression analysis builds a model that describes the cause-effect link most often using the least-square method [24], while the ANOVA evaluates the constructed model and quantifies the influence of factors and interactions on the output variable by decomposing total variance [25].

3.3. Case study DSF and experimental set-up specifications

In the context of this study, we decided to select one representative DSF configuration, i.e., a naturally ventilated DSF operating in the so-called ‘‘outdoor air curtain” mode. In this system, the ventilated cavity of the DSF receives air from the outdoor and releases air back to the outdoor. This configuration aims to reduce the solar gain through the glazing by combining the use of an in-cavity shading device (in the case study, a venetian blinds system) and ventilation airflow to remove heat from the cavity (see, e.g. [26]). This type of façade may thus operate by modulating the free cross-sectional area of the inlet/outlet sections – to control the naturally driven airflow – and by deploying the shading device (and titling the blinds) – to reduce the direct solar transmission through the façade. This operational mode and control possibility is of particular interest in the cooling season since this configuration is one

of the most adopted for improving the thermal performance during this period [27], as fully glazed envelopes usually show poorer performance [28]. Congruent with this configuration, the boundary conditions (as described more in detail in the next section) were chosen to represent situations where such DSF mode would be most helpful, i.e., conditions typical of the summer period. The characterization of the performance of such a DSF under the selected boundary conditions was carried out through a full-scale DSF mock-up installed into a climate simulator (Figs. 1 and 2). The DSF test sample was made of inner and outer double glazing incorporated into the aluminum frame. Both were composed of two glass panes with dimensions 1.4 m (W) × 2.8 m (H), and the gap between the panes was filled with a mixture of air and argon (4–15–4 mm) [17].

The measurement system consists of more than 70 sensors to measure the temperature of the surrounding environment, the air in the cavity and surface of different facade segments, incident and transmitted solar radiation, air velocity in the cavity, pressure difference, and heat flux density [17]. A dedicated system for control and monitoring of the experiment was developed in the LabView environment to monitor a large number of measurements in real-time. The characteristics of sensors that measured the physical quantities used for the assessment of the performance indicators (response variables) are given in Table 1.

The climate simulator is an indoor experimental facility with two chambers intended to replicate the indoor and outdoor environment surrounding a building envelope element. The test element needs to be installed into a large metal frame and placed between two chambers. The integrated sun simulator can replicate solar irradiance in the approximate range between 250 Wm^{-2} and just over 1000 Wm^{-2} by using an array of nine metal halide lamps. In the study presented in this paper, we controlled the cells' air temperature values and the irradiance provided by the solar simulator. The climate simulator is not capable of reproducing the effect of the dynamic pressure of wind, and hence when the airflow in the DSF's cavity was activated due to the boundary conditions, this could only be attributed to the stack effect generated in the DSF's cavity. Therefore, no other pressure source than the one thermally induced was involved in this process.

We must also point out here that due to the limitations of the climate simulator, we were not able to fully replicate desired conditions in some experimental runs. For example, the air conditioning system experiences problems controlling the temperature of the outdoor chamber when the solar simulator is active. For irradiation levels of 350 Wm^{-2}, the actual temperature is 2–3 °C, while for 700 $Wm^{-2,}$ it is 4–5 °C higher than the projected one. Furthermore, the air is not uniformly cooled through the chamber, which results in a vertical temperature gradient up to 2 °C directed upwards. The reader who is interested in obtaining more details on both the flexible DSF mock-up and the climate simulator can find this information, which is not reported here in the complete form for the sake of brevity, in a previous paper [17].

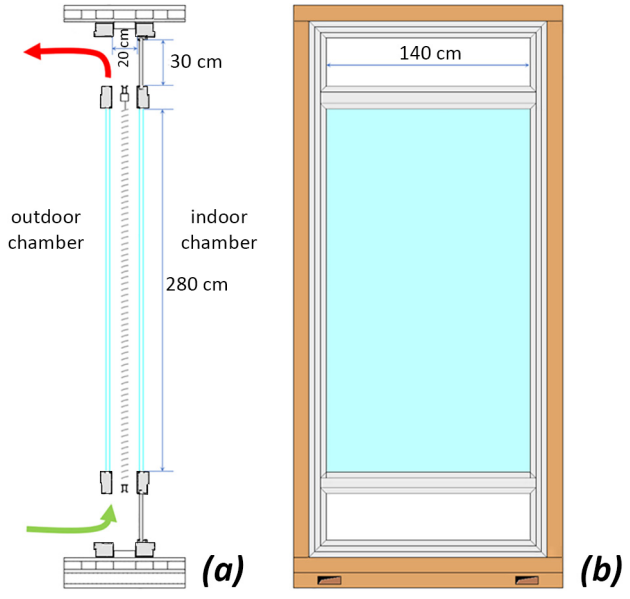

Fig. 1. Schematic representation of the DSF a) vertical section, b) front view.

3.4. Applications of the DOE methodology in the context of this study

Relevant independent variables (factors) and dependent variables (response variables) were identified considering the degree of freedom allowed by the experimental set-up and a set of interesting quantities that could be used to study the performance of the DSF. These variables and their levels are summarized in Tables 2 and 3.

The air temperature in the outdoor cell of the climate simulator was considered an important variable, and therefore different levels were adopted, while the indoor temperature was set to the constant value of 25 °C, which corresponds to a realistic indoor air temperature setpoint during the cooling period. The combination of a variable outdoor air temperature level and a fixed indoor air temperature level led to a variable temperature difference between the outdoor and the indoor environment (in the range −10 °C to + 10 °C), which we considered a relevant factor in the performance of a DSF and therefore it was investigated. In addition to this factor, solar irradiance level on the vertical plane was chosen as the second boundary condition variable, with the range 0 W/m^2 to 700 W/m^2.

The flexible mock-up allowed a large range of configurations to be tested, and in the experimental run presented in this study, the following features of the DSF were changed: the angle (0°, 45° and 90°) of white-aluminum colored venetian blinds with a solar reflectivity in the range of 0.5 to 0.6; the free cross-sectional area of the openings at the top and at the bottom of the DSF (for each opening, between 7 dm^2 and 42 dm^2, which corresponds to 500 and 3000 cm^2/m of facade width, respectively). Consideing that the focus of this study was on the operational phase of a DSF (i.e. when design decisions have already been taken and the performance is driven by how the façade is controlled), the choice of varying the only two variables that can be modified under operation seemed a fully logical choice. Furthermore, these two variables also have an impact on other domains than the thermal one (e.g. shading devices influence the light transmission through the facade, inlet/outlet opening influence the sound transmission through the façade) and their operations might therefore be based on more complex logics than just the thermophysical performance of the DSF. Undestanding what impact they have on the thermophysical performance is therefore also important in light of constructing control strategies for a dynamic DSF that trade-off against performance across different domains (e.g. when an optimized thermal performance needs to be combined with sound insulation requirements or with daylight exploitation targets).

We must emphasize that other design factors, such as the optical properties of glazing or slats, can have a significant impact on the thermal performance of DSF [29–31,12]. However, in the context of our study, we treated these as invariable elements and used a constant configuration. The selected types of glazing was, to some extent, not conventional, and a short explanation of the reason for this choice might be beneficial.

DSF are oftentimes realized with a combination of a single-glass skin and a double/triple-glazing skin. For this study we instead

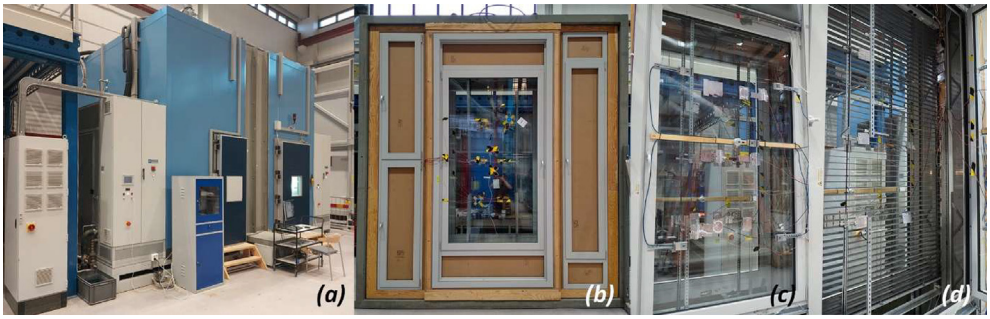

Fig. 2. Experimental set-up: (a) the climate simulator with the façade installd between the two chambers (and visible as the metal frame between the two blue cells); (b) frontal view of the DSF mock-up installed in the frame for insertion in the climate simulator facility; (c) and (d) sensors installation on the mock-up. (For interpretation of the references to color in this figure legend, the reader is referred to the web version of this article.)

Table 1
Characteristics of the sensors used in the characterization of the DSF.

Sensor type	Measured quantity	Accuracy
Pyranometer	Incident and transmitted solar irradiance	Class 2 (ISO 9060)
Hot-wire anemometer and temperature sensor	Speed and temperature of the air in the cavity	v: ±(0.1 m/s + 3 % of measured) for (0…1 m/s) and t: ±0.3 °C
Air temperature sensor	The temperature of the air near the inlet and outlet	±0.3 °C for range (0…70 °C)
Resistance temperature detector Pt100	The surface temperature of glazing and shading	Class B (from ± 0.37 °C at −10 °C to ± 0.70 °C at 80 °C)
Heat flux plate	Heat flux density through glazing	Calibration uncertainty: ± 3 %

Table 2
Factors and corresponding levels.

Factors	Symbol	Unit	Levels		
			Low	Mid	High
Solar irradiance	ISR	[Wm^{-2}]	0	350	700
Temperature difference	DBT	[℃]	−10	0	10
Venetian blind angle	SA	[°]	0	45	90
Inlet/outlet free cross-sectional area (Opening size)	OS	[cm^2m^{-1}]	500	1500	3000

opted for a double glazing unit for both the skins. The reason is that we wanted to enhance the thermal decoupling of the cavity and the inner and outer environment. In this way the intrinsic flexibility that a DSF has, i.e. to remove/store heat in the cavity thanks to the cavity airflow, can be better investigated due to lower transmission loss through the two skins compared to a conventional DSF configuration.

Another fixed construction feature that may have an impact on the extendibility of the results presented in this study is the cavity depth. Narrow cavities have recently gained preference (especially in single-floor DSFs) for a series of reasons [32–34], among them lower costs and volume, and because of this trend we opted in this investigation to fix the cavity depth to 20 cm. In addition to being a representative configuration from a market perspective, our previous studies have also shown that for the single-floor DSFs with cavity depths in the range of 20–60 cm, this feature plays a less relevant role compared to other factors in shaping the performance of a DSF [12,17]. While, in general, the cavity size (and the relative position of the shading, i.e. closer or further away from one of the two skins) can impact on the heat exchange between the shading and the glazing, we have seen that for the situation where there is a sufficient cavity depth that ensures a certain distance between the shading and the glazing, the size of the cavity and the exact position of the shading does not have a great impact. Therefore, the missing exploration of the impact of the cavity depth as an independent parameter does not represent, in our opinion, a relevant shortcoming in this study, particulary when considering that this parameter cannot be varied under operations of a DSF.

Several response quantities may be chosen to outline the thermal and fluid dynamics behavior of a DSF, and we decided to include the following in our study: the net heat flux density, the average temperature of the cavity, airflow rate, heat gain/loss rate by the airflow that passes through the cavity normalized by the DSF surface (hereafter referred to as heat gain/loss rate by the airflow), and the average surface temperature of the inner glazing. Net heat flux density represents the sum of heat flux density measured by the heat flux meter installed on the inner side of the inner glazing (q_{HFM}) and transmitted solar radiation to the interior registered by the inside pyranometer (q_{TR}). The average cavity temperature is determined based on the 12-point measurements of hot wire anemometers. The same instruments were used to assess velocity profiles and airflow rate at two heights, based on which the airflow rate is evaluated. Heat gain/loss rate by the airflow represents the heat rate absorbed or released by the airflow that passes through the cavity normalized by the DSF surface, and it is calculated based on the evaluated airflow rate and measured heating/cooling of the airflow when passing through the cavity (t_{out}-t_{inl}). The indoor surface glazing temperature represents the average temperature of the inner surface of the inner glazing measured by the surface temperature sensors.

The uncertainty of the measurements of the response quantity was assessed using the method of error propagation [35] and expressed in a range of values, from the lowest to highest error, since the error may depend on the exact conditions of the tests, and more than 50 experimental runs were done. Experimental uncertainty consists of two parts: the uncertainty originating from the instrument limitations and the error arising from the variability of the measured quantity (standard deviation). As is always the case with steady-state measurements under well-controlled conditions, the first part is dominant over the statistical error. This effect can be clearly seen in the temperature measurement results, where the experimental error belongs almost entirely to instrumental inaccuracy, though this also indicates the strictly maintained steady-state conditions in the climate chambers. It is also important to note that the airflow and heat gain/loss rateby the airflow are characterized by the high uncertainty due to the inaccuracy of hot-wire anemometers.

Table 3
Response quantities and corresponding uncertainties.

Response quantity	Symbol	Unit	Equation	Uncertainty range
Net heat flux density associated with the DSF	q_{net}	[Wm^{-2}]	$q_{HFM} + q_{TR}$	0.3 ~ 9.9
The average cavity temperature	t_{cav}	[℃]	$\bar{t}_{cav}$	0.30 ~ 0.32
The airflow rate	$\dot{V}$	[m^3h^{-1}]	Velocity profile method	101 ~ 122
Heat gain/loss rate by the airflow that passes through cavity normalized by the DSF surface	q_{vent}	[Wm^{-2}]	$\dot{m}c_p(t_{out} - t_{inl})$	3 ~ 116
The indoor surface glazing temperature	t_s	[℃]	$\bar{t}_s$	0.50 ~ 0.50

As previously mentioned, we selected four classes of experimental designs that are most often employed in engineering, where the exact features within each class were decided based on the guidelines for finding the optimal design developed in one of our previous researches [12]. The number and type of the factors and their low and high values were chosen based on the problem statement and objectives, while the complex nature of DSF behavior predetermined the minimum resolution (IV) of the design. Limitations regarding the resource demand of the physical experiments in the controlled environment dictated the maximum number of experimental runs, which in our opinion should not exceed 30. Therefore, we identified four experimental designs capable of assessing the influence of both factors and their interactions using a reasonable number of experimental runs: *Taguchi (3Lx4F), definitive screening, 2-level full-factorial, and face-centered central-composite design*. All the experimental designs were configured to cover the exact same range of variations (min value – max value) for the four factors under investigation so that they can be considered fully equivalent arrays when it comes to the domain of exploration.

The Taguchi design adopted is a fourth-order resolution design that considers not-aliased main effects and confounded two-factor interactions. It takes into account four factors with three levels using 27 experimental runs (Table 4). In comparison to this, the definitive screening design (DSD) uses just half as many experimental runs (13 runs), and it was therefore interesting to investigate its performance considering its resource efficiency. The chosen full-factorial design analyzes four factors with only two levels (low and high). In this way, the array offers, on the one hand, relatively high efficiency by having only 16 experimental runs, but on the other hand, it shows a limitation in the depth of the characterization. Our previous research [12] revealed that the face-centered type of central-composite design (CCD (α = 1)) had the best results among 30 tested experimental designs when four or five factors governed the system behavior. Therefore, we opted for the same type of array, with 25 experimental runs, and considered four factors characterized only by the central and cube points. The critical *p-value* for recognizing the statistical significance of factor/interactions in the analysis of variance and the factor selection procedures was set to 0.05 for all the designs, indicating a high probability that the considered variable is significant.

It must be emphasized here that different designs may have common points, i.e., identical configurations tested under the same conditions. This was the case in our study, where the four selected experimental designs had a series of coincident experimental runs. Since the experiments were performed in a controlled environment, where the experimental variation (noise, error) is minimal, these "repeated" experimental runs were performed only once and not separately for each different design. Therefore, the total number of experimental runs actually carried out to acquire data for all the four experimental designs was 49 instead of 81, thereby significantly reducing resource consumption. Just as is the case here, if there are enough resources, it is always wise to compare the results obtained from the ANOVA performed on two or more different experimental designs to confirm the validity of the obtained characterization picture.

In Table 5, it is possible to see, for each experimental design, the number of experimental runs that are unique and the number of those that are shared with each of the other experimental designs. We indicate the unique points along the top-left/bottom-right diagonal of the table, while shared points between different arrays are noted in the intersection of different designs. For example, FFD does not contain unique points since all other designs are derived from this array, while it shares 6 runs with TD, 4 runs with DSD, and the whole set of 16 runs of the FFD is also included in the CCD. The value in brackets refers to the percentage of runs shared between two experimental designs in cross-section of a row and column, and it measures how "unique" each experimental design is compared to the others (the lower the percentage, the more unique).

3.5. Data analysis

Upon performing the entire sequence of experimental runs that constitutes all the four experimental designs, the analysis of variance (ANOVA) was performed for each different experimental design with the aim of:.

1) comparing the characterization pictures obtained from different arrays,

2) obtaining a general picture of the performance of the façade, and

3) understanding the role of the factors and their interactions.

The overall thermal and fluid dynamic behavior was represented through assessed contributions of each factor and interaction on the variability of the different performance indicators. This quantity was calculated based on the ANOVA procedure,

Table 4
Characteristics of chosen experimental designs.

Experimental designs	Number of runs	Number of factors	Number of levels	Model
Taguchi (3Lx4F)	27	4	3	2-FI
Definitive screening design	13	4	2/3	Quadratic
Full factorial design	16	4	2	2-FI
Central composite design	25	4	2/3	Quadratic

Table 5
Unique points and shared points for different combinations of experimental designs. Unique points can be read along the main diagonal of the table (i.e., unique points for TD(3Lx4F) are 16, for DSD are 6, for FFD 0, and for CCD 5), while in all the other cells the number of shared points between the two designs can be read, with the percentage indicated between brackets.

Experimental designs	Number of runs	TD (3L×4F)	DSD	FFD	CCD
TD (3Lx4F)	27	16 (59%)	3 (11%)	6 (22%)	9 (33%)
DSD	13	3 (23%)	6 (46%)	4 (31%)	5 (38%)
FFD	16	6 (38%)	4 (25%)	0 (–)	16 (100%)
CCD	25	9 (36%)	5 (20%)	16 (64%)	5 (20%)

where the sum of squares for the factor or interaction ($SS_{F\&I}$) of interest is divided by the total sum of squares SS_T:.

$$c_{F\&I} = \frac{SS_{F\&I}}{SS_T} 100$$

where F&I is a particular factor A, B, C, D... or interaction between AB, AC, AD..., ABC, ABD...

In order to identify and quantify the similarity between two characterizations obtained with different experimental designs, we have employed a comparison method based on the *fitting coefficient f*, which we introduced in our previous study [12]:.

$$f = 1 - \frac{\sum_{F\&I} \left| c_{F\&I,RD} - c_{F\&I,D} \right| + \left| \frac{SS_{E,RD}}{SS_{T,RD}} - \frac{SS_{E,D}}{SS_{T,D}} \right|}{2}$$

The coefficient measures how much the contributions of factors/interactions ($c_{F\&I}$) and randomness (SS_E/SS_T) differ between two designs (RD – referent and D – design to be compared). The value of *f* varies from 0 to 1, where one corresponds to the absolute identity between the two characterizations, while zero indicates complete disagreement between the two characterizations.

Factorial and interaction plots were used to understand how factors and their interactions affect the behavior of DSF. The main effects (factorial) plot shows the mean response of dependent quantity for each factor level connected by a line, while the interaction plot shows how the relationship between the response variable and a factor depends on the value of a second factor. More information on this, as well as on the ANOVA calculation procedures and method for comparison of designs, one can be found in one of our previous research studies [12].

4. Results and discussion

4.1. Performance of the different experimental designs

The comparison of the different experimental designs showed an excellent agreement in terms of the characterizations of the thermal performance, carried out using the net heat flux density Q_{net}, the average temperature of the cavity t_{cav}, and the indoor surface glazing temperature t_s. All experimental designs estimated almost equal shares in the total variance with low error (Fig. 3). Only the response of the indoor surface glazing temperature fitted from DSD deviated slightly from the corresponding response obtained from FFD and CCD, but even in these cases, the match between the different designs can be considered very good (Table 6). There were also differences in whether certain designs see particular factors or interactions as statistically significant, but the contribution of these variables was very small to substantially influence the thermophysical behavior of DSF (Fig. 3). The factors' impact was dominant in influencing the cavity and indoor surface glazing temperature, and therefore linear models containing only main effects would be suitable to describe the response of these quantities. However, that was not the case with net heat flux density, where the influence of interaction between irradiance and slat angle was nearly dominant as the individual influence of factors. Therefore, models containing higher-order terms are needed to adequately fit this quantity's response.

As opposed to the thermal, fluid dynamic characterization showed more significant discrepancies, especially regarding the airflow rate assessment. For example, there were notable differences in impact assessment of different factors between the FFD and other experimental designs (Table 6). Compared to other designs, the FFD recognized the different contributions of the solar irradiance and temperature difference and did not see the statistical significance of the slat angle (Fig. 3). Most likely since two-point designs cannot fit the non-linear response of output quantity (in this case, the airflow rate V), as explained more in detail in 3.3. Every experimental design led to a simple linear model that contained only the main effects to fit the response of the airflow rate (Fig. 3). This result may raise some questions knowing that the underlying nature of the airflow is, in general, non-linear. Since all the arrays had errors higher than 5 %, it was challenging to recognize the statistical significance of non-linear terms. One may question if this result derives from the phenomenon being mostly linear in the range of investigation, or from the levels used in the investigations not being suitable, or from some other reason. Since the levels/sample points have shown to be suitable for the other indicators, there are no particular reasons to hypothesize that they were not suitable for unveiling the behavior of the airflow rate. We rather understood the large error as linked to the high measurement uncertainty in the airflow rate measurement since hot-wire anemometers could not register velocities below 0.1 ms^{-1}. Additionally, uncertainty was also associated with determining the airflow direction when the temperature difference between the fluid and the interface was less than 0.5 °C. As a result, the airflow variations below a certain threshold could not be registered by the hot-wire anemometers, resulting in a low resolution for the characterization of this phenomenon, regardless of the employed experimental design.

The resemblance between different experimental designs regarding heat gain/release by the airflow Q_{vent} ranged from very good to excellent, which was slightly worse compared to thermal performance quantities, but better than for the airflow rate (Table 6). All four experimental designs recognized the same factors/interactions as the most relevant, and these were the two boundary conditions (temperature difference and solar irradiance). Errors were more acceptable than in the case of the airflow rate but still considerably high (>5%) for some experimental designs, such as TD and DSD (Fig. 7). Due to the considerable error in those designs, the slat angle and opening size (free cross-sectional area) were not recognized as statistically significant in controlling heat absorbed/released through the airflow for a tested range of configurations and boundary conditions. The uncertainty associated with the threshold of hot-wire anemometers was most likely felt here, but to a lesser extent, as the variance of this quantity was less influenced by the low-velocity variations (check equation, Table 3). Like the net heat flux density, the response of the heat gain/release by the airflow is fitted best by a model containing higher-order terms. The interaction between solar irradiance and the temperature difference plays an important role in controlling this quantity response.

Generally speaking, it is possible to see that the differences between the four experimental designs were minor, and this indicates that all of the selected designs could sample the most representative points within the domain. More importantly, the fact that different experimental designs returned a very robust picture about the role of the different factors can be understood as a confirmation that the outputs of the analysis truly described (minus any experimental error) the thermal and fluid-dynamics behavior of the DSF. Based on this conclusion, we could therefore determine with a good degree of confidence which factors and interactions were significant and to what extent they controlled the heat transfer and the fluid flow in the DSF.

The comparison of the ANOVA performed on the different experimental designs showed that the experimental design must be capable of assessing the impact of higher-order terms to adequately characterize the behavior typical of dynamic facades. In addition to this, it is highly desirable to use designs that allows factors to have more than two levels so that the fitted model (such as quadratic) can capture curvature in the response of the dependent variable. However, it is important to emphasize that the success of the DOE characterization depends to a great extent on the uncer-

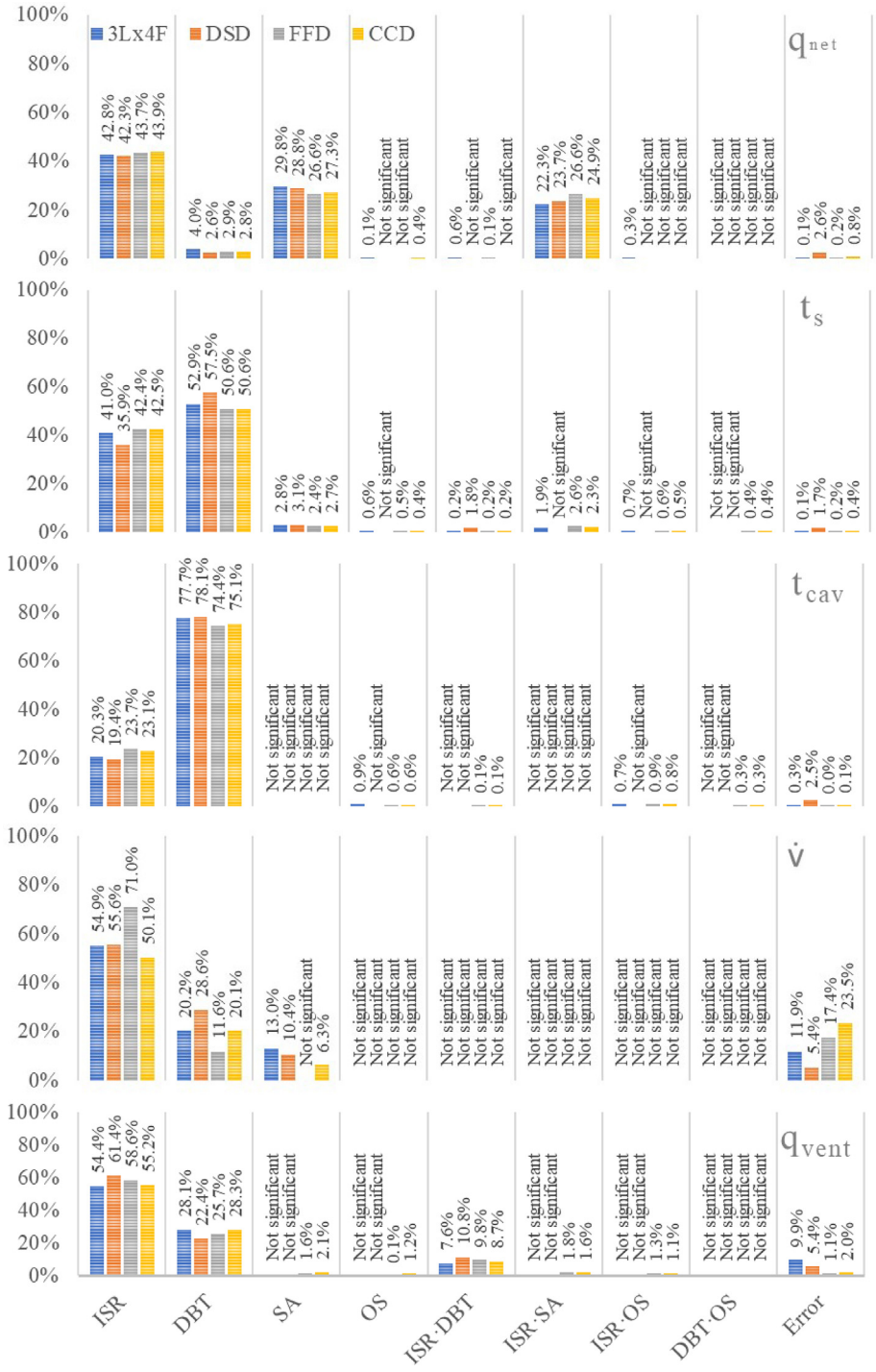

Fig. 3. Comparison of characterization of thermal and fluid-dynamic behavior of DSF obtained by different experimental designs.

Table 6
Fitting coefficient values between four different experimental designs.

	The fitting coefficient [–]					
	TD vs DSD	TD vs FFD	TD vs CCD	DSD vs FFD	DSD vs CCD	FFD vs CCD
Q_{net}	0.96	0.95	0.95	0.95	0.97	0.98
t_{cav}	0.97	0.96	0.97	0.94	0.95	0.99
t_s	0.92	0.97	0.97	0.89	0.90	0.99
q	0.91	0.78	0.88	0.73	0.82	0.79
Q_{vent}	0.90	0.89	0.92	0.92	0.88	0.95

tainties associated with the experimental campaign, even if a suitable experimental design is chosen. In a case where the variability of the response quantity was measured or determined in a less accurate way because of the challenge to measure a physical quantity (such as it was the case for air velocities below 0.1 ms^{-1}) or because of the use of a less reliable measurement method, the experimental uncertainty propagates throughout the ANOVA results, and the results coming from this process will, in the end, be less reliable. Furthermore, a large error can be caused if unsuitable factors are introduced into the analysis (e.g., interdependent factors) or desired boundary conditions are not met in the experimental procedure.

4.2. Overall thermal and fluid-dynamic behavior of a naturally-ventilated DSF

The net heat flux density of the DSF in outdoor air curtain ventilation mode was shown to be controlled almost entirely by solar irradiance and the venetian blinds, where the interactions among these two also played an essential role. Therefore, the position of the blinds in response to the incoming solar radiation clearly showed potential in controlling the heat transfer in the DSF, and hence in control of the energy efficiency of DSFs. The ANOVA results confirmed the expected prevalence of heat transfer induced by incoming solar radiation over the transmission driven by the temperature difference between indoor and outdoor environments. Therefore, the impact of solar irradiance was shown to impact the dependent variable with a weight far greater than temperature difference.

The temperature at the indoor-facing surface of the inner skin can be used as a proxy for potential thermal discomfort issues, as it impacts the mean radiant temperature of the indoor space and may contribute to local discomfort phenomena (such as radiant asymmetry). The surface temperature is almost entirely regulated by solar irradiance and the temperature difference solely, while the slat angle and the size of the opening have negligible influence. Most likely, the high insulation glazing properties decouple the cavity from the indoor surface when it comes to heat transfer. Therefore, control of accumulated heat and the airflow in the cavity by changing the slat angle and size of the opening has a minor effect on the temperature of the indoor facing surface of the glazing.

Since the air inside the cavity was in direct contact with (i.e., originated from) the outdoor air, the ANOVA indicates that the average temperature of the cavity was highly impacted by the temperature difference, more precisely by the outdoor air temperature (as the indoor air temperature was kept constant). The influence of solar irradiance was also noticeable, and similarly, as for the previous indicator, the boundary conditions were the only ones that regulated the air temperature in the cavity. The results of the ANOVA did not identify the slat angle as a significant factor that impacted the cavity air temperature, and the free cross-sectional area was also shown to be negligible. That may seem contrary to our preconceptions, but we must point out that the configuration with active shading was tested by changing only the blind angle. The shading device itself certainly influenced the temperature of the cavity by absorbing incoming solar radiation but changing only the blind angle on an already lowered shading device did not have a significant effect as it redistributed accumulated heat in the cavity while average temperature did not change significantly. Moreover, the high reflectivity of the venetian blinds with white aluminum color most likely reduced the heat accumulation and air temperature increase in the cavity. From a control perspective, this means that neither changing the angle of venetian blinds nor the percentage of the inlet and outlet opening vents (in the tested range) seemed to be an effective way to control this quantity. However, we need here to highlight that the analysis was carried out by combining boundary conditions and control features, and the results showed that boundary conditions have a much greater impact on the dependent variable(s). This effect might "hide", in the ANOVA, the effect of the control features, which could still be non-negligible given a specific set of boundary conditions. Parametric experiments where only the control variable (i.e. slat angles of the blinds or free cross sectional area of the inlet/outlet) is changed and boundary conditions are kept constant could possibly to identify the effect of each control variable given a certain solicitation.

The airflow generated in the DSF's cavity was generated only due to the stack effect, as this could be the only driving force to activate a flow (considering that the climate simulator could not replicate, for example, the effect of the wind). Hence, we considered the heat transfer due to temperature difference across the DSF's domain and the heat gain due to solar irradiance as the two reasons for a temperature stratification within the DSF's cavity. The ANOVA analysis showed that the airflow in the cavity was triggered more by the solar irradiance than the temperature difference, which was something we had expected. The first factor, especially in the summer period, provides the DSF with higher heat gain and thus generates larger temperature differences between the air in the cavity and the surrounding boundaries, thereby contributing to stronger natural convection. Changing the slat angle modified the amount of absorbed radiation and consequently the temperature difference to the surrounding air and thus most likely affected natural airflow in the cavity. The smallest size of the opening was probably big enough to create pressure drops comparable to the one generated by the largest size, so the effect of changing aperture size was not significant. We can hypothesize that further reducing the inlet/outlet opening size (hence the free cross sectional areas) would reduce airflow, which would be felt more significantly since the DSF would gradually switch to another operational mode (air buffer).

Heat gain/loss associated with the airflow plays a vital role in the thermal load relief of a DSF ventilated by the outdoor air curtain means in the summer. As mentioned, the solar irradiance generated a stronger heat gain/release by the airflow than the temperature difference, though the former factor also played an important role since the cavity was in direct contact with the outdoor air. The solar radiation prevalence comes from the fact that the radiative processes are largely responsible for the accumulation of the heat in the cavity and the generation of the airflow rate. Similar to the cavity temperature, it is expected that installing the venetian blinds induces heat absorption/release by the airflow and its diversion toward the outside. However, changing only the slat angle on an already deployed shading device did not play a significant role. Since the ANOVA results showed that the opening size did not significantly affect the airflow in the cavity, it was expected that the impact of the same factor was not recognized as statistically significant for the heat absorbed/released by the airflow.

Summing up, the results of the characterization showed that the thermal performance of the tested configuration in the summer period was governed primarily by the boundary conditions, and to a lesser extent, by the slat angle of venetian blind as a structural/-operational parameter. That was especially true for indoor surface glazing and cavity temperatures, where the temperature difference played a dominant role. These variables could hardly be controlled by changing the slat angle or the size of the vent opening. On the contrary, by modifying the reflected, absorbed and transmitted solar radiation, the shading device angle was crucial in controlling net heat flux density. Since the inlet/outlet opening size did not significantly affect the airflow generation in the cavity, its influence on other response quantities was not recognized by the results of the ANOVA. The airflow in the cavity was induced by the solar radiation more than the temperature difference, while

the slat angle helped control its rate, but to a limited extent. The predominance of solar irradiance compared to the temperature difference was also notable in heat gain/release by the airflow, but unlike the airflow rate, changing the slat angle had a negligible impact on this response quantity.

From this picture it seems that some response variables could not be significantly modified through construction variables (the slat angle and the size of the vent opening), at least compared to natural drivers (boundary conditions) in the given range of boundary conditions and tested configurations. Here, again, we can propose as a reasonable explanation for this evidence that larger variations of these response quantities are possible at the design stage, where optical and thermal properties of the glazing and the shading device can be selected over a large range of possibilities, but once these are fixed, the variation allowed by the operational factors are limited. Of course, such results may depend on the choice we made for the specific test case (in terms of glazing types and shading type, especially when it comes to their optical properties), though the selected configuration for the unchangeable factors was done bearing in mind a realistic case scenario.

4.3. Assessment of main effects and interaction effects

4.3.1. Factor impact analysis

The different designs generally identified a linear response of net heat flux density to all factors, and thus we can conclude that experimental designs that use only two points can be almost as successful in modeling the response of the net heat flux density as those that use more than two points. On average, the increase in solar irradiance led to a rise in neat heat transfer, while opening the blinds led to an increased transmitted solar radiation and thus to an amplified net heat flux density – two results that are not surprising (Fig. 4 – 1a). The impact of the temperature difference was not as strong as the solar irradiance and slat angle when it comes to the net heat flux density (Fig. 4 – 1b). However, this factor showed similar linear behavior as the two previously mentioned parameters, where lower temperatures (than those inside the interior) suppressed the net heat flux density, while the higher ones induced it (Fig. 4 – 1c). The response of the output quantity to changes in the free cross-sectional areas of the inlet/outlet (vents' opening size) showed certain features of non-linearity, where the middle-sized point had the most optimal outcome in reducing net heat flux density (Fig. 4 – 1d). However, just a small error would be made if the effects of non-linearity were neglected since it was shown that the cross-sectional area did not strongly influence either the airflow or the heat absorbed/released by it in the ventilated cavity.

The way factors affected the indoor surface glazing and cavity temperature was similar to the net heat flux density, where on average, the increase in solar radiation and temperature difference led to a linear rise of considered response quantities (Fig. 4 – 2a, 2b, 3a, and 3b). CCD recognized a certain extent of non-linearity in cavity temperature response to temperature difference and opening size (2b and 2d), but these effects were negligible. The same is notable for the indoor surface glazing temperature response to alteration in the slat angle and the opening size (3c and 3d).

As expected, solar radiation and temperature difference induced the airflow in the cavity, while thermal equilibrium and conditions with no radiation tended to diminish it (Fig. 4 – 4a and 4b). All designs except FFD point to the considerable non-linear response of the airflow rate to changes in temperature difference, which must be taken into account to obtain the correct characterization picture (Fig. 4 – 4b). FFD does not account for this non-linearity, and therefore the weaker effect of temperature difference on airflow rate was approximately two times greater than for the other three designs (Fig. 3). The airflow rate response fitted from the FFD might erroneously indicate that the airflow rate weakens as the outdoor temperature rises. On the contrary, RS, DS, and Taguchi 3Lx4F designs imply that the absence of a temperature difference dampened the airflow in the cavity, which is much more physically grounded. The gradual closure of the venetian blinds led to an increase in the airflow rates, which is expected as the temperature difference between slats and surrounding fluid also increases, leading to the intensification of natural convection (Fig. 4 – 4c). Due to the high error, none of the models saw opening size as the significant factor in controlling airflow rate (Fig. 4 – 4d). As stated before, the inability of designs to adequately fit airflow rate response originates from the limitations of the measurement technique and the underlying non-linear nature of air dynamics in the cavity.

In general, there was a linear response of heat gain/loss rateby the airflow to changes in solar irradiance and the temperature difference (Fig. 4 – 5a and 5b). However, it is interesting that solar radiation and outdoor temperature exerted opposite effects on the heat gain/release by the airflow (Fig. 4 – 5a and 5b). Generally, the amount of absorbed heat by the airflow decreased with increasing outdoor temperature, which is different from the concave-shaped response of the airflow rate with a minimum at medium temperature (0 °C temperature difference). Therefore, we can conclude that the amount of heat removed by the airflow toward the outside decreases as the ambient temperature increases. The CCD indicated particular non-linearity in response to the slat angle and opening size, implying that the highest quantity of removed heat (by the airflow) corresponds to the closed blind and mid-size opening (Fig. 4 – 5c and 5d).

Factors impact analysis showed that the heat transfer and natural convection gradually intensified while temperatures of construction DSF elements linearly rose with the increase of solar irradiance. Similarly, an increase in outdoor temperature led to a linear rise of both indoor glazing surface and cavity temperature and net heat flux density. In contrast, the amount of heat removed from the cavity by the airflow decreased linearly as the temperature difference increased from negative to positive. Non-linear, concave-shaped airflow response to temperature difference was recorded without clearly defined minimum, but with notable feature indicating largest airflows for negative temperature differences. Opening venetian blinds (0° to 90°) led to the rise of the heat entering the indoor environment and the temperature of the indoor glazing surface. In contrast, the same act caused attenuation of the airflow and the amount of heat removed by it from the cavity, although to quite a bounded extent for the latter response quantity. Although the vent opening size had shown a very limited range of influence, some traces of its action on response quantities could be glimpsed in the factorial plots. The CCD recognized that the mid-size opening had the most optimal impact on the net heat flux density reduction and the amount of heat removed from the cavity by the airflow. Furthermore, reducing the opening size led to the increased temperatures of the indoor glazing surface and the air in the cavity.

4.3.2. Interaction impact analysis

The main effects described the airflow rate and cavity temperature response, while for all other response quantities, interactions were needed to characterize the thermophysical behavior of the DSF correctly. Therefore, interactions played a significant role in controlling processes in the DSF, and hence, the main effects could not be interpreted without considering them. Since many statistically significant interactions were not decisive in controlling DSF performance, we will consider only those with the highest contribution share. The analysis outcome showed that the interaction between solar irradiance and the slat angle (in regulating net heat flux density) and the interaction between solar irradiance and tem-

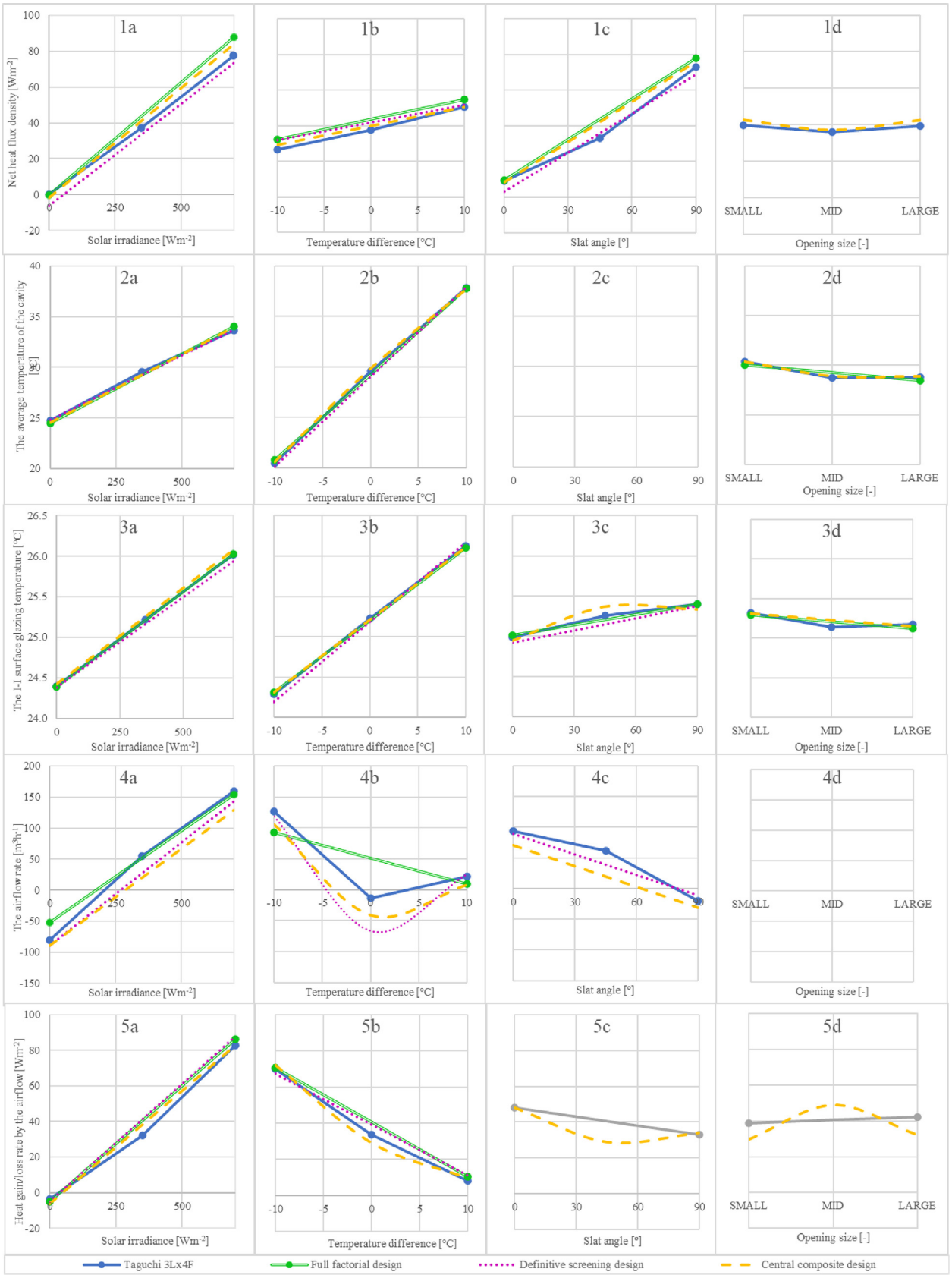

Fig. 4. Analysis of the influence of factors on neat heat transfer, the average air temperature of the cavity, the indoor surface glazing temperature, the airflow rate, and heat gain/loss rateby the airflow (from top to bottom, respectively). The responses to statistically non-significant factors seen by various experimental designs resulted in an empty chart (see graphs 2c and 4d) or a chart that with an almost flat profile (see graphs 1d, 2d, 5c, and 5d). The responses fitted by the quadrature models (DSD and RASD) do not contain markers, unlike those fitted from the 2-FI models (TD and FFD).

perature difference (in controlling heat gain/release by the airflow in the cavity) were the significant interactions to consider.

The net heat flux density response to a combination of solar irradiance and the slat angle, fitted from Taguchi 3Lx4F and FF designs, is shown in Fig. 5. The plot indicates the importance of the slat angle in controlling net heat flux density when there is a non-null value of solar irradiance. Shifting the angle from 90° (open position) to 0° reduced, on average, the net heat transfer by seven times while changing from 45° to 0° (closed position) resulted in a reduction by around three times. Furthermore, combining a medium level of solar irradiance (~350 Wm^{-2}) and open slats produced approximately the same net heat flux density as for high solar radiance level (~700 Wm^{-2}) and 45° opened blinds. The interaction plot does not differ significantly between FFD and Taguchi 3Lx4F designs for opened and closed blinds. However, we could not achieve insight into the combined effect of half-closed blind and solar irradiance relying only on the FFD.

Fig. 6 shows the interaction effect between solar irradiance and temperature difference on heat gain/loss brought by the airflow in the cavity, where a negligible heat gain/release by the airflow in the absence of solar irradiance is notable. When the outside air temperature was colder than the indoor air temperature combined with a medium or a high solar of solar irradiance (>350 Wm^{-2}), the airflow absorbed large quantities of heat accumulated in the cavity. The amount of heat removed from the cavity and transported towards the outdoor environment decreased as the outside temperature rose. The combination of medium solar irradiance (~350 Wm^{-2}) and the medium and high outdoor air temperature (from 25 °C to 35 °C) emphasized this effect. Following the same situation as the previous case, it is impossible to obtain insight into the combined effect of a null temperature difference and solar irradiance with FFD due to the limitations characterizing this design. Finally, we can conclude that ventilating a DSF with an outdoor air curtain is not recommended during hot periods (35 °C) combined with no or medium radiation levels (~350 Wm^{-2}) since the airflow removed no heat, or the heat was even released to the boundaries of the cavity. The interaction plots obtained from the CCD and DSD indicated similar features as those retrieved from Taguchi and FFD, so we decided to omit the former to make the graphics easier to read.

Interaction effects can be analyzed from the contour and surface plots for experimental designs that use quadratic models, such as DSD and CCD. The fitted response of net heat flux density as a function of solar irradiance and the slat angle can be seen in Fig. 7a (for DSD) and 6b (for CCD). In each chart, the surfaces parametrically depict the net heat flux density response to solar irradiance and the slat angle as a function of constant values of the other statistically significant factors. In Fig. 7a (concerning DSD) surfaces represent net heat flux density response to solar irradiance and slat angle as a function of constant temperature difference, while in Fig. 7b (concerning CCD), surfaces depict the same response as a

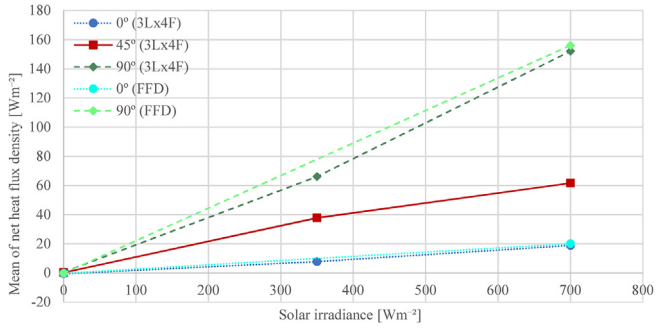

Fig. 5. Effects of interaction between solar irradiance and the slat angle on net heat flux density.

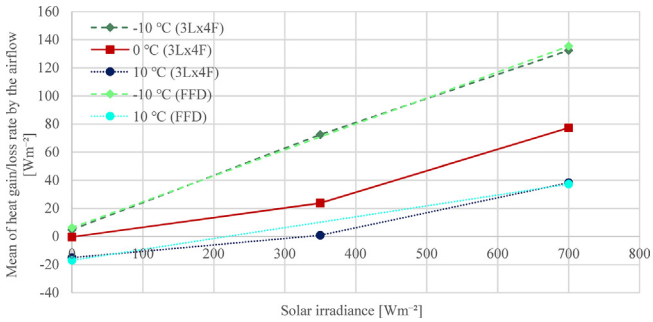

Fig. 6. Effects of interaction between solar irradiance and the slat angle on heat gain/loss rate by the airflow.

function of combined constant temperature difference and opening size.

In Fig. 7a and 7b, one can see that the slat angle played the dominant role in controlling the net heat flux density by blocking solar radiation from being transmitted in the interior. For example, having closed slats substantially limited the effect of alteration in solar irradiance. By closing the venetian blinds (from 90° to 0°), the reduction factor for a net heat transfer increased multiple times, depending on the value of solar irradiance. The thickness of the stacked surfaces in Fig. 7a, 7b, and 8b indicates the variations range of the response quantity caused by the significant factors held at the constant level. Considering this, it is visible from Fig. 7a that the temperature difference had a considerably weaker impact on the net heat flux density than solar irradiance or the slat angle. Similar is notable in Fig. 7b for the combined influence of temperature difference and the opening size. Parallel surfaces visible in Fig. 7a and 7b point to the type of interaction between the solar irradiance and the slat angle, which is the same for any temperature difference (Fig. 7a) or any combination of the temperature difference and the opening size (Fig. 7b).

Fig. 8a and 8b depict the heat gain/release (by the airflow) response to the temperature difference and the solar irradiance fitted from DSD and CCD. Both figures indicate similar behavior, with the DSD showing only one surface since no statistical significance other than solar irradiance and temperature difference was recognized. In addition to two dominant factors, the quadratic model fitted from CCD recognized the statistical significance of the slat angle and the opening size. Therefore, in Fig. 8b concerning CCD, surfaces represent the response of the heat gain/release by the airflow to the temperature difference and the solar irradiance as a function of combined constant slat angle and the opening size. From the given figure, one can detect the optimal configuration for heat removal by the airflow from the cavity in certain environmental conditions. For example, in situations that correspond to high solar irradiance and outdoor temperature difference (700 Wm^{-2}, 35 °C), closed blinds and mid-size openings produced six times higher heat removal by the airflow than the combination of opened blinds and small opening size. For conditions that suit high solar irradiance and low outdoor temperature, that effect is less amplified (700 Wm^{-2}, 15 °C), with an increase of around 50%. Unlike in Fig. 7a and 7b, surfaces intersect, which means that the temperature difference interacted with solar irradiance in different ways for different combinations of the slat angle and the opening size. Like the interaction plots, surface plots indicate the negative effect of the outdoor air curtain ventilation mode in periods without solar irradiance and with high outdoor temperature. The highest amount of diverted heat towards the outside was for a combination of high radiation and cold outside temperature. Under these conditions, the enthalpic gain of the ventilation airflow was about 2.5 to 3.5 times greater than in the case of both high outside air temperature and a high level of solar irradiance.

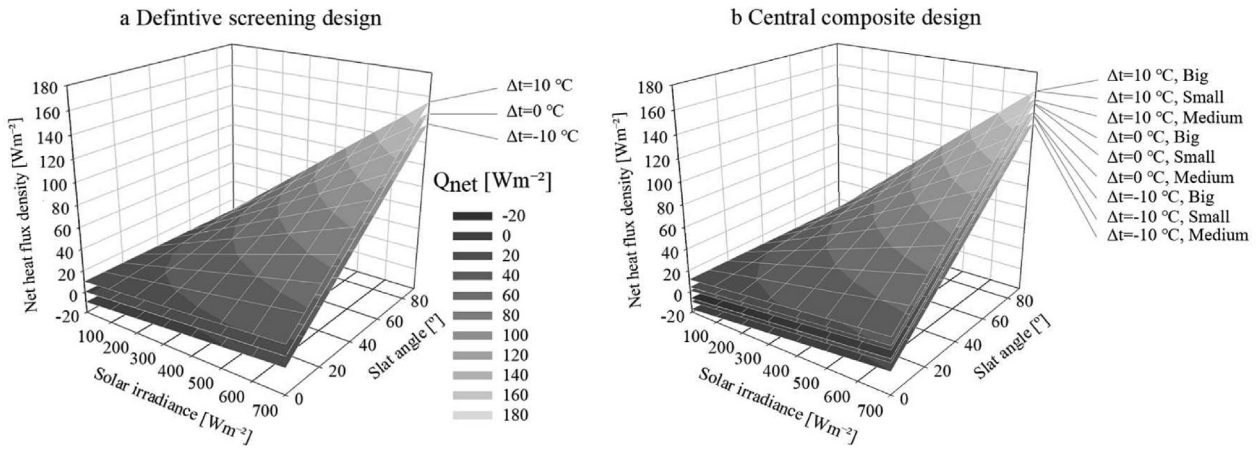

Fig. 7. The surface plot of the net heat flux density response to solar irradiance and the slat angle fitted from the DSD (left) and CCD (right).

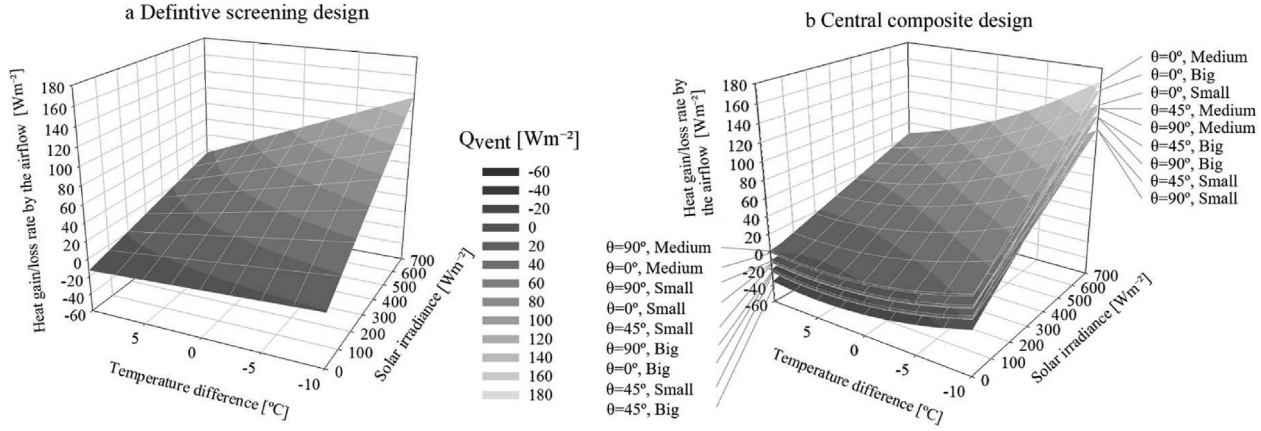

Fig. 8. The response of heat gain/release rate by the airflow to the temperature difference and the solar irradiance fitted from the DSD (left) and CCD (right).

Interactions played a significant role in controlling DSF performance, especially when it comes to the net heat flux density and the amount of heat absorbed/released by the airflow passing through the cavity. The solar radiation impact on the heat entering the indoor environment was significantly reduced with closed blinds. For high radiation levels, shutting the blind from completely open to closed led to a reduction of net heat flux density up to seven times. The highest heat amount removed by the airflow from the cavity was present in replicated conditions of high solar irradiance and cold outdoor temperature (15 °C). In situations corresponding to the absence of solar irradiance and high outdoor temperature (35 °C), the airflow passing through the cavity released the heat to the surrounding boundaries, while in the same thermal conditions and with medium solar irradiance level, the airflow hardly removed any heat from the cavity.

5. Conclusions

The application of DOE methodology in building energy and thermal performance research is not a novel concept, but almost all studies involve simulations rather than physical experiments. With this research we aimed to contribute to the knowledge on how to apply DOE methodology successfully to experiments in a controlled environment and choose an optimal experimental design suitable for the characterization of complex systems.

In our analysis we employed and compared four experimental designs able to assess higher-order terms and non-linear behaviors typical of a DSF. The depictions of thermal behavior obtained from different experimental designs resemble each other excellently, while the somewhat weaker agreement between arrays was found for the fluid dynamics. However, even in this case, the resemblance was satisfactory, which enabled us to deduce which factors affect, and in what way, heat transfer and air dynamics in the cavity.

We can conclude what characteristics an array needs to have to provide a sufficient characterization picture of the cause-and-effect relationships between variables in the complex process of a DSFs, and by extension, in other complex processes seen in building science:.

- Experimental design needs to adequately estimate the impact of higher-order terms in order to characterize the behavior of complex systems, such as dynamic facades, adequately. The main effects in such systems can not be interpreted without considering interactions.
- Designs should be able to assess the non-linear response of the output quantity. Therefore, arrays should either fit a quadratic model or have a minimum of three points so that 2FI-models can recognize deflection in the response.
- The unexplained variance needs to be as low as possible, preferably less than 5%, so the statistical significance of interactions and weaker terms can be recognized. If we suppose optimal experimental design is chosen for characterization, an error larger than 5 % indicates possible irregularities in planning or performing the experiment. For example, the experimenter can

select the factors that are not mutually independent, or in the experimenting phase, there may be problems in maintaining the desired boundary conditions. Furthermore, a high error can be caused by the limitations (inaccuracies) of the used instrumentations or the unreliability of the experimental method, where all these experimental uncertainties will propagate to the results of the ANOVA.
- If there are enough resources, it is always wise to compare the results obtained from the ANOVA performed on two or more different experimental designs to confirm the validity of the obtained characterization picture. That is often feasible since many experimental designs share common points and the total number of experimental runs for two different array may be less than the sum of the experimental run for each individual array.

In addition to comparing the performance of different experimental designs, this research aimed at deepening the understanding of the behavior and the quantification of the thermopysical phenomena (and to what extent they can be controlled) in naturally ventilated DSFs, operating in outdoor air curtain mode, under typical summer conditions. The characterization of these processes was performed using a climate simulator system and an on-purpose developed façade mock-up. Construction and operational features of both the climate simulator and the mock-up may have impacted the results and limited their full extendibility to in-field cases. It is therefore necessary to consider the following aspects while going through the conclusions of our study.

The climate simulator was able to replicate the conditions in which the airflow in the cavity was driven only by the buoyancy, and thus the effect of the wind as an environmental factor is not considered. Most likely, the DSF performance will depend to a greater extent on the inlet/outlet opening size if the effects of wind are taken into consideration as an additional driving factor.

From a measurement perspective, it should be emphasized that the characterization of fluid-dynamic behavior through quantities such as the airflow rate or heat gain/loss by the airflow contained a considerable amount of uncertainty accumulated through the limitations of the velocity profile method and inaccuracy of hot-wire anemometers. The nature of the test facilty, however, makes it complicated to select alternative techniques for monitoring the airflow, and other options that are (at least on the paper) more promising than the velocity profile method for low airflow rates (e.g. [36]), might not be suitable for this test setting.

The tested facade mock-up was a single-story DSF, which we considered representative of current trends in the construction of adaptive facades that prefer compact prefabricated elements. However, there are other types, such as the shaft-box or multi-story DSF, where stronger buoyancy effects may result in a different picture when it comes to the processes assessed in this study. Moreover, some of the factors that influence the global performance of a DSF, such as the optical characteristics of glazing or shading, were not treated as variables in this study, but we adopted fixed elements that we considered suitable to study the problem of the control of a DSF under (peak) summer-time boundary conditions.

In focusing our study on control variables (opening size of the inlet/outlet section; tilt angle of the venetian blind), it was easy to set the range for the venetian blinds (from fully closed to fully open), while a much greater degree of freedom was left in choosing the range for the opening size. The results of the impact of the free cross-sectional area on the controllability of some phenomena might therefore be linked to the selected range for this variable, and different (notably, smaller) values of the free cross-sectional area might have led to a different picture (i.e. that this variable too could play a more relevant role when one can modulate the free cross-sectional area down to 100 to 200 cm^2/m of facade width).

Based on the outcomes of the characterizations obtained from different experimental designs, we can draw the following conclusions for our specific façade mock-up, which we believe are realistically extendable to a larger range of single-story naturally ventilated DSFs.

- Boundary conditions are central regulators of the thermal and airflow behavior of a DSF, and the range in which DSF behavior can be impacted by adjusting the operational features (i.e., the shading devices and the free cross-sectional area) can be very limited for some performance parameters (i.e., convective gains of the airflow in the cavity, the indoor glazing surface, and cavity temperatures).
- However, certain aspects of energy performance can be efficiently controlled by manipulating the features of the DSF, such as net heat flux density through the control of the slat angle. Finding the optimal position of the lamellae in response to solar irradiance is beneficial to optimize the energy efficiency of a DSF, as transmitted solar radiation represents, on average, the largest share in the net heat flow.
- Buoyant flow in the cavity with installed venetian blinds is driven far more by the solar irradiance (absorption of solar radiation by the DSF components) than by the temperature difference between outdoor and indoor environments.
- The highest airflow rates are observed for the combination of high solar irradiance and negative air temperature difference (colder outdoor temperature compared to the internal one).
- The slat angle can control the airflow to a limited extent, where the gradual closing of blinds leads to intensifying the mass flow rate in the cavity.
- The highest amount of heat removed by the airflow from the cavity is found in conditions corresponding to high radiation levels and outdoor air temperatures lower than internal ones. We can conclude that the amount of accumulated heat in the cavity diverted toward the outside by the outdoor air curtain is reduced with increasing outdoor temperature and decreasing solar irradiance, making it a ventilation mode with a moderate or litttle effect in periods like hot nights or hot cloudy days.

Similar conclusions about the importance of venetian blind slat angle in controlling heat entering the indoor environment have been obtained as in the studies [37–39] with a similar reduction factor for closed slats [37]. Experimental and CFD investigations [38,40,41] found likewise that gradual closure of the blind leads to the enchantment of naturally induced airflow and heat removed from the cavity. Unlike most research that evaluates the individual (parametric) influence of constructional features in clearly defined conditions, this study addressed the different configurations' influence in a range of boundary conditions typical for the most critical period for DSF performance. As such, a broader view was given of the extent to which the thermal and fluid dynamic behavior of a DSF can actually be controlled under summer conditions.

As a final note, in an effort to make our research data freely accessible and to allow maximum usability of the collected experimental characterisations, all the measurements presented in this study have been uploaded to on an open-access repository. Data can be found at, and referenced using, the following weblink: https://doi.org/10.5281/zenodo.6187723 [42].

Declaration of Competing Interest

The authors declare that they have no known competing financial interests or personal relationships that could have appeared to influence the work reported in this paper.

Acknowledgements

The activities presented in this paper were carried out within the research project "REsponsive, INtegrated, VENTilated - REINVENT – windows", supported by the Research Council of Norway through the research grant 262198, and the partners SINTEF, Hydro Extruded Solutions, Politecnico di Torino and Aalto University. The authors would like to thank M. Salman Siddiqui and Odne Oksavik for their support in developing the software for control and data acquisition. The technical partner Hydro Extruded Solutions (Hydro Building Systems) is also gratefully acknowledged for its support in developing and engineering the flexible mock-up and the in-kind contribution for its construction.

References

[1] A. Jankovic, F. Goia, Impact of double skin facade constructional features on heat transfer and fluid dynamic behaviour, Build. Environ. 196 (2021) 107796.
[2] J. Antony, 2 – Fundamentals of Design of Experiments, J. B. T.-D. of E. for E. and S. (Second E. Antony, Ed. Oxford: Elsevier, 2014, pp. 7–17.
[3] J.K. Telford, A brief introduction to design of experiments, Johns Hopkins Apl Tech. Dig. 27 (2007) 224–232.
[4] M.A. Farooq, H. Nóvoa, A. Araújo, S.M.O. Tavares, An innovative approach for planning and execution of pre-experimental runs for Design of Experiments, Eur. Res. Manag. Bus. Econ. 22 (3) (2016) 155–161.
[5] C.F.J. Wu, M.S. Hamada, A systematic approach to the planning and implementation of experiments, in: Experiments: planning, analysis, and optimization, 2nd ed., John Wiley & Sons, New Jersey, 2009, pp. 4–8.
[6] H. Guo, A. Mettas, Design of experiments and data analysis, in: 2010 Reliability and Maintainability Symposium, 2010, pp. 1–11.
[7] N. Delgarm, B. Sajadi, K. Azarbad, S. Delgarm, Sensitivity analysis of building energy performance: a simulation-based approach using OFAT and variance-based sensitivity analysis methods, J. Build. Eng. 15 (2018) 181–193.
[8] A.N. Sadeghifam, S.M. Zahraee, M.M. Meynagh, I. Kiani, Combined use of design of experiment and dynamic building simulation in assessment of energy efficiency in tropical residential buildings, Energy Build. 86 (2015) 525–533.
[9] A. Schlueter, P. Geyer, Linking BIM and Design of Experiments to balance architectural and technical design factors for energy performance, Autom. Constr. 86 (2018) 33–43.
[10] W. Kim, Y. Jeon, Y. Kim, Simulation-based optimization of an integrated daylighting and HVAC system using the design of experiments method, Appl. Energy 162 (2016) 666–674.
[11] R. Evins, P. Pointer, R. Vaidyanathan, S. Burgess, A case study exploring regulated energy use in domestic buildings using design-of-experiments and multi-objective optimisation, Build. Environ. 54 (2012) 126–136.
[12] A. Jankovic, G. Chaudhary, F. Goia, Designing the design of experiments (DOE) – An investigation on the influence of different factorial designs on the characterization of complex systems, Energy Build. 250 (2021) 111298.
[13] X. Shen, G. Zhang, B. Bjerg, Assessments of experimental designs in response surface modelling process: estimating ventilation rate in naturally ventilated livestock buildings, Energy Build. 62 (2013) 570–580.
[14] I. Jaffal, C. Inard, C. Ghiaus, Fast method to predict building heating demand based on the design of experiments, Energy Build. 41 (6) (2009) 669–677.
[15] N.R. Smalheiser, Chapter 5 – Experimental Design: Design Strategies and Controls, N. R. B. T.-D. L. Smalheiser, Ed. Academic Press, 2017, pp. 65–85.
[16] B.H. Margolin, Resolution IV fractional factorial designs, J. R. Stat. Soc. Ser. B 31 (3) (1969) 514–523.
[17] A. Jankovic, M.S. Siddiqui, F. Goia, Laboratory testbed and methods for flexible characterization of thermal and fluid dynamic behaviour of double skin facades, Build. Environ. 210 (2022) 108700.
[18] L. Ilzarbe, M.J. Álvarez, E. Viles, M. Tanco, Practical applications of design of experiments in the field of engineering: a bibliographical review, Qual. Reliab. Eng. Int. 24 (4) (Jun. 2008) 417–428.
[19] B. Durakovic, Design of experiments application, concepts, examples: state of the art, Period. Eng. Nat. Sci. 5 (3) (2017) 421–439.
[20] G. Box, S. Bisgaard, C. Fung, An explanation and critique of taguchi's contributions to quality engineering, Qual. Reliab. Eng. Int. 4 (2) (1988) 123–131.
[21] K.N. Ballantyne, R.A. van Oorschot, R.J. Mitchell, Reduce optimisation time and effort: Taguchi experimental design methods, Forensic Sci. Int. Genet. Suppl. Ser. 1 (1) (2008) 7–8.
[22] W. Libbrecht, F. Deruyck, H. Poelman, A.n. Verberckmoes, J. Thybaut, J. De Clercq, P. Van Der Voort, Optimization of soft templated mesoporous carbon synthesis using Definitive Screening Design, Chem. Eng. J. 259 (2015) 126–134.
[23] S. Karimifard, M.R. Alavi Moghaddam, Application of response surface methodology in physicochemical removal of dyes from wastewater: a critical review, Sci. Total Environ. 640–641 (2018) 772–797.
[24] D.C. Montgomery, The regression approach to the analysis of variance, in: Design and analysis of experiments, 9th ed., John Wiley & Sons, New York, 2017, pp. 119–123.
[25] H.C.J. Hoefsloot, D.J. Vis, J.A. Westerhuis, A.K. Smilde, J.J. Jansen, in: 2.23 - Multiset Data Analysis: ANOVA Simultaneous Component Analysis and Related Methods, Elsevier, Oxford, 2009, pp. 453–472.
[26] F. Favoino, Assessing the performance of an advanced integrated facade by means of simulation: The ACTRESS facade case study, J. Facade Des. Eng. 3 (2) (2015) 105–127.
[27] T. Hong, J. Kim, J. Lee, C. Koo, H. S. Park, Assessment of seasonal energy efficiency strategies of a double skin façade in a monsoon climate region, *Energies*, 6 (9). 2013.
[28] I.-A.-E.-K.-M. Amaireh, Numerical investigation into a double skin façade system integrated with shading devices, with reference to the city of Amman, University of Nottingham, Jordan, 2017.
[29] A. Guardo, M. Coussirat, E. Egusquiza, P. Alavedra, R. Castilla, A CFD approach to evaluate the influence of construction and operation parameters on the performance of Active Transparent Façades in Mediterranean climates, Energy Build. 41 (5) (2009) 534–542.
[30] H. Choi, Y. An, K. Kang, S. Yoon, T. Kim, Cooling energy performance and thermal characteristics of a naturally ventilated slim double-skin window, Appl. Therm. Eng. 160 (2019) 114113.
[31] J.P. Varughese, M.M. John, Effect of emissivity of shading device and air flow inside cavity of Double Skin Facade for energy saving and Thermal Comfort in buildings: A CFD modeling, in: *2016 International Conference on Energy Efficient Technologies for Sustainability, ICEETS 2016*, 2016, pp. 815–820.
[32] G. He, L. Shu, S. Zhang, Double skin facades in the hot summer and cold winter zone in China: cavity open or closed?, Build Simul. 4 (4) (2011) 283–291.
[33] N. Safer, M. Woloszyn, J.J. Roux, Three-dimensional simulation with a CFD tool of the airflow phenomena in single floor double-skin facade equipped with a venetian blind, Sol. Energy 79 (2) (2005) 193–203.
[34] A. Hazem, M. Ameghchouche, C. Bougriou, A numerical analysis of the air ventilation management and assessment of the behavior of double skin facades, Energy Build. 102 (2015) 225–236.
[35] J.P. Holman, Uncertainty Analysis and Propagation of Uncertainty, in: Experimental Methods for Engineers, 8th ed., McGraw-Hill/Connect Learn Succeed, New York, N.Y., 2012, pp. 63–72.
[36] A. Jankovic, G. Gennaro, G. Chaudhary, F. Goia, F. Favoino, Tracer gas techniques for airflow characterization in double skin facades, Build. Environ. 212 (2022) 108803.
[37] D. Iyi, R. Hasan, R. Penlington, C. Underwood, Double skin façade: Modelling technique and influence of venetian blinds on the airflow and heat transfer, Appl. Therm. Eng. 71 (1) (2014) 219–229.
[38] Y. Ji, M.J. Cook, V. Hanby, D.G. Infield, D.L. Loveday, L. Mei, CFD modelling of naturally ventilated double-skin facades with venetian blinds, J. Build. Perform. Simul. 1 (3) (2008) 185–196.
[39] X. Hong, M.K.H. Leung, W. He, Effective use of venetian blind in Trombe wall for solar space conditioning control, Appl. Energy 250 (Sep. 2019) 452–460.
[40] V.I. Hanby et al., Nodal network and CFD simulation of airflow and heat transfer in double skin facades with blinds, Build. Serv. Eng. Res. Technol. 29 (1) (2008) 45–59.
[41] L. Mei et al., The influence of blinds on temperatures and air flows within ventilated double-skin facades, in: *Proceedings of Clima 2007 WellBeing Indoors*, 2007, p. 1606.
[42] A. Jankovic, F. Goia, An experimental data set for the analysis of the thermophysical behavior of a single-story naturally ventilated double-skin façade (DSF) under summer boundary conditions, 2022. [Online]. Available: 10.5281/zenodo.6187723.